Journal of Applied Fluid Mechanics, Vol. 17, No. 11, pp. 2448-2464, 2024.
Available online at www.jafmonline.net, ISSN 1735-3572, EISSN 1735-3645.
https://doi.org/10.47176/jafm.17.11.2709

CFD Investigation of Dual Synthetic Jets on an Optimized Aerofoil's Trailing Edge

R. Srinath [1,2†], R. Mukesh [3], I. Hasan [3] and P. R. Krishnan [3]

[1]*Department of Aerospace Engineering, R V College of Engineering, Bangalore 560100, India*
[2]*Department of Aeronautical Engineering, Visvesvaraya Technological University, Belagavi, Karnataka, India*
[3] *Department of Aerospace Engineering, ACS College of Engineering, Bangalore 560074, India*

[†]*Corresponding Author Email: srinathr@rvce.edu.in*

ABSTRACT

In fluid dynamics, a flow control device is used to control, manage, or modify the behavior of a fluid flow. Jet actuators work by releasing high-velocity jets of fluid, usually air or gas, into the surrounding environment to control or manipulate the flow of fluids. In this study, the flow control device, which was a dual synthetic jet actuator (DSJA), acted as a lift enhancement device over an optimized NACA 0012 aerofoil with a rounded trailing edge (TE) (Coanda surface approximately 9% of the trailing edge was modified) to enhance the lift at various angles of attack (AOAs). Fluctuating pressure inlets were introduced in two slots. When the dual synthetic jets were in control, the out-of-phase jets from the upper and lower trailing edge jets helped to boost the lift coefficient. The suction stroke from the lower half of the jet made the Coanda effect stronger in the upper half. The upper trailing edge jet deflected downwards merged with the lower one and helped to deflect the flow field closer to the bottom half. An unsteady CFD analysis was performed on optimized airfoils with and without a DSJ, with a driving frequency of 40.6 and a reduced frequency of 0.025 at a Reynolds number of 25000. The results obtained at different angles indicated that the L/D ratio was improved by 13.5% at higher angles of attack in the presence of the DSJA.

Article History

Received March 8, 2024
Revised May 16, 2024
Accepted May 22, 2024
Available online September 1, 2024

Keywords:

Synthetic jets
Coanda effect
Unsteady CFD analysis
Aerodynamic efficiency
Antiphase jets

1. INTRODUCTION

In the pursuit of improved aircraft performance and efficiency, various researchers have promoted innovative strategies to enhance the lift generation. A commercial airplane's fuel costs could be decreased by 8% if it was possible to delay the transition process on its wing to 50%. Among the various techniques used, the utilization of flow control devices has evolved to improve the aerodynamic characteristics. For a longer period of time, flaps are considered prominent high-lift devices, giving rise to increments in lift and an increase in aerodynamic efficiency(Kumar & Kumar, 2013). Traditional lift enhancement devices, such as flaps of different types and other devices, have contributed significantly in enhancing the lift up to a certain angle of attack (Kumar & Kumar 2013; Setyo Hariyadi et al., 2023). However, at critical angles, the flow splits closer to the trailing edge, which then picks up the energy and maximizes the wake region and moves to the leading edge. This transition typically happens when the airplane is flying at a low Reynolds number (Re), where laminar flow is more common (Yang et al., 2023). When adverse pressure gradients (APGs) become significant, the boundary layer can detach from the surface (Serdar Genç et al., 2020). The separation of the flow and adverse pressure gradients reduces the efficiency to a greater extent at higher angles of attack. Flow separation can be delayed, which in turn increases the stall angle, by introducing flow control techniques. Flow control devices encompass a spectrum of technologies, ranging from passive devices, such as vortex generators and winglets, to active systems such as plasma actuators and synthetic jet actuators (Ali & Fales, 2021). The integration of these devices aims to minimize the drag, delay the stall, and ultimately amplify the lift forces, contributing to a more efficient and sustainable aviation landscape (Moshfeghi & Hur, 2014; Larbi et al., 2020). Passive control devices focus on an additional mechanical surface that alters the flow, thereby reducing the flow separation at higher angles of attack. Conversely, active devices depend on external power to achieve the same effect (Hares et al., 2019). This works seeks to improve the flow separation and stall angle delay of an optimized NACA 0012 aerofoil with active flow control surfaces.

In the field of aerodynamics, the augmentation of the lift through innovative flow control devices is required to

NOMENCLATURE

A	amplitude	f^+	reduced frequency
A_0	maximum amplitude	l	characteristic length
AOA	Angle Of Attack	M_{Jet}	mass of jet
AR	Aspect Ratio	NACA	National Advisory Committee for Aeronautics
CAD	Computer-Aided Design	OQ	Orthogonal quality
CC	Circulation Control	RANS	Reynolds-averaged Navier–Stokes equations
C_D	coefficient of drag	T E	Trailing Edge
CFD	Computational Fluid Dynamics	U_∞	free stream velocity
CL	coefficient of lift	V_{Jet}	velocity of jet
C_P	coefficient of pressure	ρ_{Jet}	density of jet
DSJA	Dual Synthetic Jet Actuator	ω	angular frequency
f	frequency		

improve the cost efficiency and achieve weight reductions. From leading-edge slats to self-activated deployable flaps, passive devices initially played a unique role in influencing aerodynamic performance (Traub & Kaula, 2016). A few decades later, Gurney flaps and roughness materials were introduced as effective passive control techniques. The usage of passive vortex generators and, their mechanisms, contributed valuable insights to the evolving landscape of lift enhancement in aviation (Siddiqui & Chaab, 2021). However, circulation control (CC) eases the actuation and thereby increases the life coefficient without additional mechanical components. The CC methods, unlike passive ones, actively manage the airflow around the aerofoil (Kweder et al., 2010). These devices, typically embedded within the wing structure, strategically blow high-velocity jets of air at specific points. Active circulation control is an evolving technology with undeniable potential. It has the ability to revolutionize airplane design and improve the performance of wind turbines and drones (Kweder et al., 2010; Liu et al., 2022; Wang et al., 2023). They are categorized as jets, which simply use compressed air to directly inject high-velocity jets into the boundary layer. Synthetic jet actuators create the illusion of a jet without actually expelling air (Mankbadi et al., 2015). Gul et al. (2014) found that periodic activation from synthetic jet actuators removed the laminar separation bubble over the upper surface of the aerofoil at a Reynolds number of $2.3x10^5$ and at zero angle of attack (AOA). Synthetic jets are created through the motion of a flexible membrane, within an enclosed space, rather than through traditional nozzles or fluid-expelling jets (Ja'fari et al., 2023). The DSJA presented, in the current study uses two such oscillating chambers that work in tandem. These pulsating jets are directed towards the aerodynamic surface, producing localized changes in the airflow. Plasma actuators use high-voltage electric fields to ionize the air (Neretti, 2016), creating tiny jets of plasma that manipulate the airflow. Benard et al. (2008) revealed that a (DBD) plasma actuator is a simple and effective active device for flow control that imposes momentum on the boundary layer by operating at a high frequency, without any mechanical components or the addition of weight. The use of jets and plasma jets involves the activation of actuators to create a controlled flow of air and prevent the separation of the flow. These methods eliminate the need, to expel a mass of air, allowing them to achieve zero net mass flux (ZNMF). The jets or the flow energize the boundary layer, preventing it from thinning and detaching, maintaining a smooth airflow and boosting the lift (Kweder et al., 2010; Neretti, 2016). Fluid blown as a part of CC adds momentum to the airflow, efficiently increasing the lift generated by the aerofoil (Djojodihardjo & Thangarajah, 2014). This allows for better lift at subordinate speeds or higher angles of attack, improving the take-off and landing performance (Ball et al., 2008). By streamlining the airflow and preventing separation, active circulation control can also minimize the drag and increase the fuel efficiency (Naqvi, 2006).

The concept behind CC is based on the Coanda effect. It refers to the tendency of a jet flow to trail a body without separating from it or immediately detaching when exposed to a moving stream of fluid. This effect arises due to pressure differences, the viscosity, and the shape of the surface (Mamou & Khalid, 2007). However, the thick trailing edge (TE) (deformed to meet the needs of the Coanda effect) of the CC aerofoil creates drag, which limits the aerodynamic performance improvement. The flow separation bubbles are greatly reduced, which enhances the aerodynamic efficiency (Li et al., 2022). In aerospace, the Coanda effect is able to refine the lift and maneuverability of an aircraft, as evidenced by studies such as (Mamou & Khalid, 2007). Moreover, in fluid dynamics and fluidic control systems, the Coanda effect plays a crucial role in directing the fluid flow, with applications in the design of fluidic thrust vectoring systems, as explored in (Schwagerus et al., 2023). Numerous research works indicate that the standalone application of the Coanda surface on an aerofoil yields minimal or negligible effects (Moshfeghi & Hur, 2014). Typically, the Coanda effect affects the flow path without causing significant changes in the pressure or velocity values along the suction surface. Studies highlight that the Coanda effect is effective when combined with a jet flow (Zhang et al., 2012). Research (Moshfeghi & Hur, 2014) demonstrates that introducing a jet flow near the leading edge of an aerofoil yields promising results in altering the flow patterns, while its proximity to the trailing edge enhances the aerodynamic efficiency. Experimental and numerical works carried out using two synthetic jets; one near the leading edge and another closer to the trailing edge emphasize the effectiveness of a Coanda double-jet configuration in controlling the boundary layer flow separation (Zhang et al., 2022). In the current study, the impact of dual synthetic jets (DSJs), both situated closer

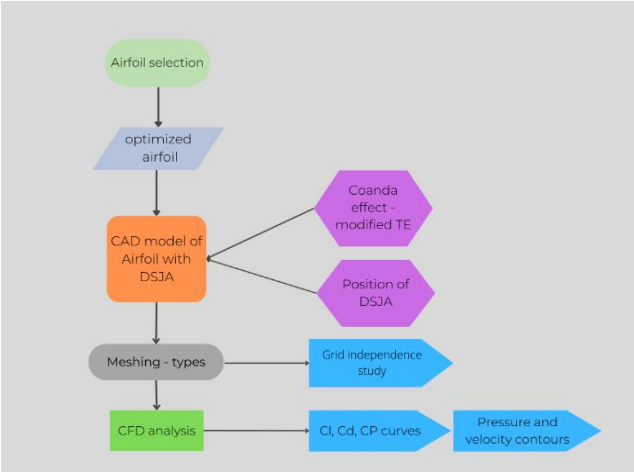

Fig. 1 Methodology followed for optimization of aerofoil

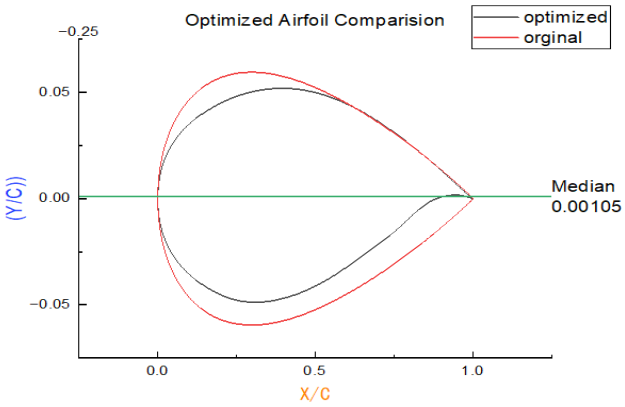

Fig. 2 Original and optimized NACA 0012 aerofoil using SLQP

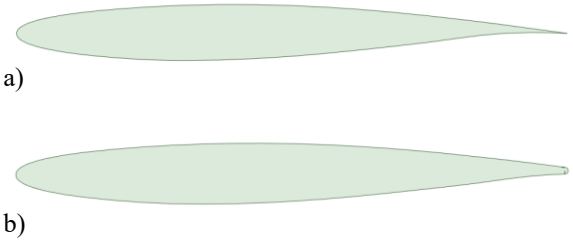

Fig. 3 CAD model of the a) optimized aerofoil (baseline) and b) trailing edge modified optimized aerofoil

While DSJAs address flow control through exciting jets, the Coanda effect influences the trajectory of the airflow. This combined approach, utilizing the instantaneous control capabilities of DSJAs and the persistent influence of the Coanda effect, results in a comprehensive enhancement in the aerodynamic efficiency and performance in critical flight conditions.

2. METHODOLOGY

The methodology is carried out as shown in Fig. 1.

A suitable aerofoil profile, NACA 0012, is selected to improve its application in the field of wind turbines and the empennage of aircraft. The primary focus of the work is the application of a DSJA as a control device to enhance the lift; however, it is essential to acknowledge the integral role of the optimized aerofoil in this study. The aerofoil was shape-optimized as shown in Fig. 2, to reduce the drag coefficient via constraints on the lift by employing the Sequential Least Squares Quadratic Programming (SLSQP) technique (Hoppe, 2006), ultimately enhancing its aerodynamic characteristics. Initially, a baseline mesh and free-form deformation (FFD) points were generated. The aerofoil geometry was defined using Bezier curves (Shikhar Jaiswal, 2017) through pyGeo, using the initial design variables. CFD tools were used to simulate the flow over the modified mesh, utilizing an AD flow, while the geometric constraints were computed using pyGeo. The optimizer updated the design variables based on the total derivatives computed with the adjoint computation module, leading to a series of iterative processes (Mukesh et al., 2012; Gibert Martínez et al., 2021). This iterative approach ensures the achievement of an optimized aerofoil design. Although the work highlights the effectiveness of DSJAs, the optimized aerofoil provides a crucial basis for the achievement of better aerodynamic performance. The trailing edge of the aerofoil was modified to utilize the benefits of the Coanda effect

The CAD model of the original and optimized aerofoils without the DSJ (considered as the baseline aerofoil in this paper), as illustrated in Fig. 3a and 3b, was created to perform the computational analyses. Three aerofoil models are mentioned in this paper, as follows: i) the original NACA 0012 aerofoil (obtained from the UIUC database), ii) the optimized aerofoil (baseline aerofoil obtained through optimization), and iii) the optimized aerofoil integrated with the DSJ and with a modified trailing edge. The chord length of the aerofoil was $c = 300\ mm$, and 9% of the trailing edge was modified, as shown in Fig. 4. The ratio of the Coanda radius (r) to the chord length was 1.6% on the trailing edge. The slot height (h) to chord length ratio was defined as 1‰ (h / c = 1%). The CFD analysis was conducted in two stages: pre-processing and post-processing (Choudhari et al., 2021).

The CAD model of the baseline aerofoil was redesigned to position the jet actuators in the opposite direction, as indicated in Fig. 4. The mutually perpendicular synthetic jet actuators sprayed the fluid, enhanced the momentum of the liquid, and delayed the flow separation. Both actuators were controlled by the piezoelectric diaphragm for practical purposes. The upper jet, or the first jet, sprayed the fluid on the upper surface of the aerofoil and the lower one on the lower surface. The jet sprayed from jet 1 increased the circulation over the upper surface, and the fluid moved as per the designed Coanda surface, whereas the lower one created a flap-like arrangement and allowed the flow to move closer to the trailing edge.

The free stream velocity (U) was 40 m/s, and the Reynolds number chosen for the numerical analysis was approximately 25000. Following the pre-processing procedure, the performance metrics of the optimized aerofoils with and without the DSJ were evaluated using

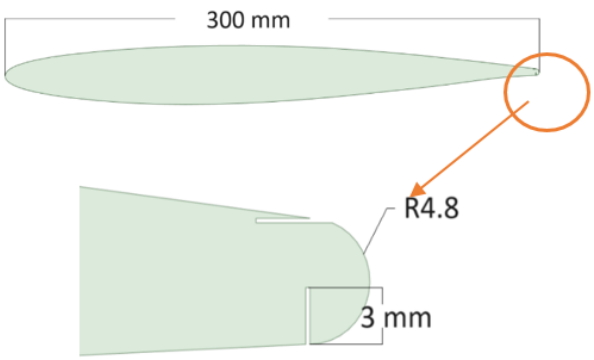

Fig. 4 CAD model of the trailing edge modified aerofoil with DSJ

post-processing. When the desired output was achieved and the performance met the requirements, the analysis was concluded. The coefficient of pressure (C_P), coefficient of lift (C_L) and coefficient of drag (C_D) against the AOA curves were extracted via post- processing (Chumbre et al., 2018). The C_P vs. X/C curves of both aerofoils provided clarity on the results, which were later compared with those of the aerofoil without the DSJA, to determine the performance improvement.

2.1 Dual Synthetic Jet Actuators and Coanda Effect

DSJAs are based on the principle of synthetic jet propulsion. They produce an airflow through episodic motion or elastic membrane within a cavity named a diaphragm (Dahalan et al., 2015). The conventional nozzles and continuous blowers expel the fluid to the surroundings and energize the boundary layer. Unlike these, a DSJA does not spill fluid but relies on the structural motion of the device. A DSJA involves two synthetic jet sources in proximity, each with a chamber and an oscillating diaphragm driven by electrical or mechanical forces (Zhao et al., 2016). This periodic motion creates pressure fluctuations, causing the displacement of the fluid, resulting in the ejection and retraction of the fluid from the chamber, as shown in Fig. 5. The Coanda effect, refers to the situation in which the boundary layer of the fluid aligns itself with a curved surface. The contribution of this effect in an aerofoil, is to enhance the lift. During the design of aerofoils, the trailing edges are modified to generate the effect by which the fluid bends over the curved surface of the aerofoil to induce an increased pressure gradient. By using this effect along with a DSJA, the flow over the aerofoil can be modified to enhance the aerodynamic performance (Ahmed et al., 2017).

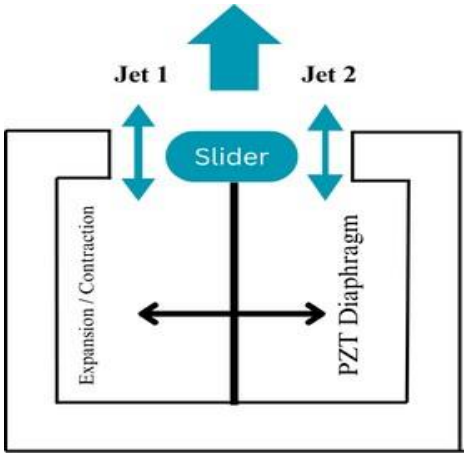

Fig. 5 Working of a dual synthetic jet actuator

2.2 Meshing

The analyses carried out to explore the characteristics of an unsteady flow over an aerofoil, both with and without the use of DSJs, through computational fluid dynamics (CFD) simulations. The work carried out emphasized the critical role of meshing in obtaining accurate and reliable unsteady aerodynamic behavior. In this regard, various meshing strategies were explored, including an O grid, C grid, and regular grid types (Aqilah et al., 2018), referring to Fig. 6. a, b, c, to identify the most suitable one. The computational domain for meshing uses quadrilateral, nonoverlapping control volumes. Adequate grid clustering allows one to observe the turbulence and viscous effects closer to the wall. The crucial parameters, such as the orthogonal quality and aspect ratio, were identified, and a mesh domain with superior orthogonal quality and a finer aspect ratio was selected for further analysis. This selection ensured a solid foundation for the post-processing and in-depth exploration of the influence of the DSJA on the aerofoil's performance. This provided a clear understanding of the aerodynamic implications of the unsteady flow dynamics and highlighted the importance of meshing strategies. Fine grid sizing was used for meshing throughout the analyses, which yielded a Y^+ value of 0.7. The coarse type of mesh was initially applied, which yielded a higher value of Y^+, being more than 3. A linear difference was noticed with a fine and coarse grid. The coarse type of grid did not fulfil the needs of the $k\ \omega\ SST$ model. As the Y^+ value required to solve the problem is less than 1.

The meshing analysis involved three types of mesh domains, namely: a C grid, O grid, and box grid, with the corresponding details shown in Table 1.

The O grid was chosen for further study. The O grid configuration, demonstrated an OQ of 0.48, indicating a higher level of orthogonality compared to the C grid (OQ of 0.37) and the box grid (OQ of 0.44). The OQ is a crucial factor that directly impacts the accuracy of fluid dynamics representation in computational fluid dynamics (CFD) simulations. A higher OQ indicates the better alignment of the grid lines with the flow direction. The O grid also exhibited an almost ideal aspect ratio of 1.000002, signifying a well-balanced distribution of element sizes within the mesh. The aspect ratio plays a pivotal role in determining the quality of a mesh, with lower values indicating a more uniform distribution of elements.

3. COMPUTATIONAL PARAMETERS

For the simulation, the flow field defined by the 2-D unsteady Reynolds-averaged Navier- Stokes equation

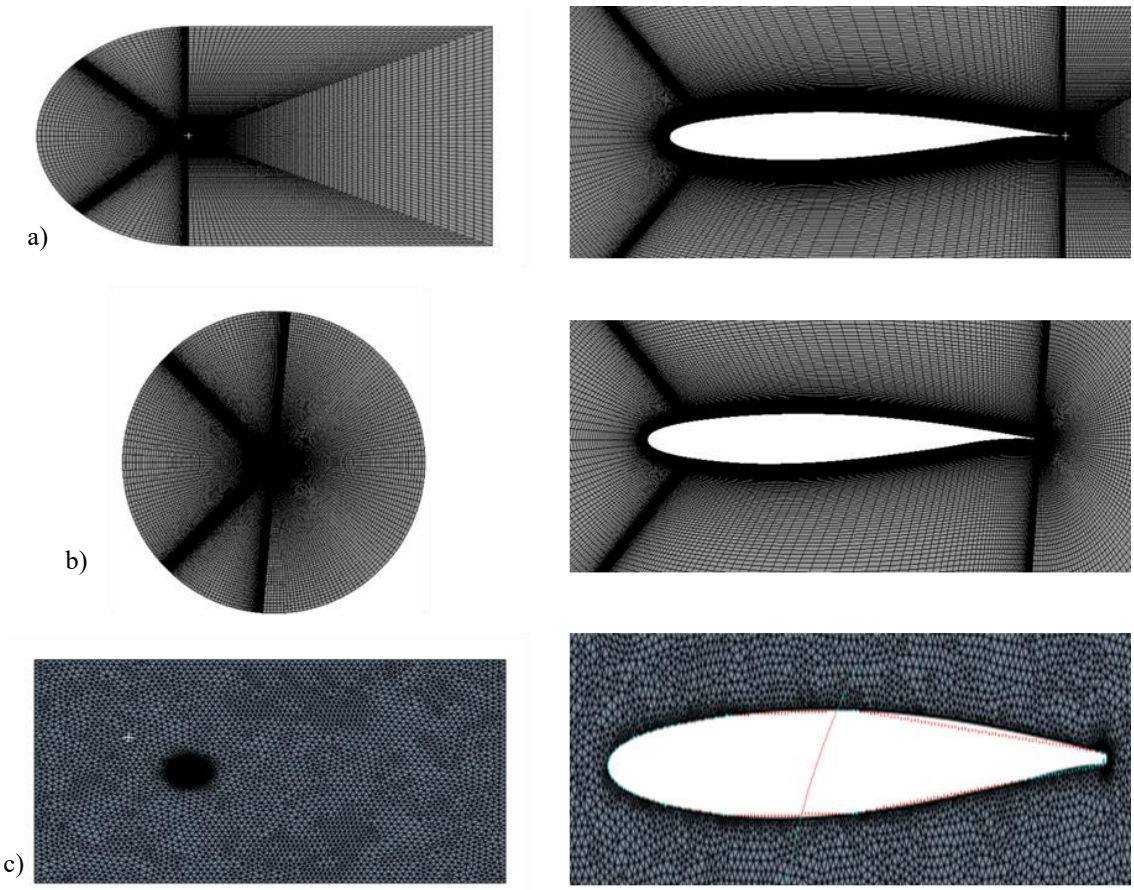

Fig. 6 Various types of meshing: a) C type, b) O type, c) box or rectangular type

Table 1 Comparison of quality of domain with mesh elements and its type

Type of mesh	No. of elements	Type of element	Orthogonal quality	Aspect ratio
C grid	449865	Quad	0.37	1.008
O grid	425896	Quad	0.48	1.000002
Box grid	435863	Tetra	0.44	1.0005

(URANS equation) was used (Khan et al., 2020). The calculations in this study were performed using the SIMPLE solver in the Fluent software, chosen for its robust handling of fluid dynamics calculations. The viscous, turbulence model, the k−ω SST model (Ou et al., 2018; Zhang et al., 2018), shown in Eq. 1, was employed. This model, is known for its accurate simulation of circulation control. The boundary conditions included a no-slip condition on the aerofoil's surface to accurately simulate the fluid interaction and a pressure far-field condition on the outer boundary to emulate the distant fluid environment. Numerically, a second-order upwind difference scheme was adopted for spatial discretization, and a second-order implicit scheme was used for time advancement, enhancing the precision and stability of the simulation by capturing detailed and dynamic changes in the flow field.

$$\frac{\partial(\rho U_i)}{\partial t}+\frac{\partial(U_iU_j)}{\partial x_1}=-\frac{\partial P}{\partial x_1}+\frac{\partial}{\partial x_j}\left[\mu\left(\frac{\partial U_i}{\partial x_j}+\frac{\partial U_j}{\partial x_1}\right)-\rho u_i'u_j'\right] \quad (1)$$

The turbulence model, the k−ω SST, uses a blending function that combines the advantages of the two turbulence models. The k-omega model is vulnerable to the free stream values. The k-epsilon turbulence model provides better compatibility in these cases. Hence, a blending function is preferred to shift from the k-epsilon model away from the wall (free stream region) to the k-omega model close to the wall.

3.1 Experimental Validation

To ensure the reliability of the numerical solutions, an experimental study was conducted on the baseline aerofoil in a subsonic suction-type open-circuit wind tunnel, as shown in 7.a. The inlet of the wind tunnel fed the fluid to a settling chamber provided with five anti-turbulence screens to remove any non-axial rotating components of the flow, before passing to the bell mouth nozzle. The details of the tunnel are given in Table 2.

The presence of honeycombs, helps in creating a smooth laminar flow with turbulence of less than 1% in the test section. A 3D printed model of the baseline aerofoil was used in the test section, as seen in 7.b. The distribution of the coefficient of pressure (C_P) from CFD was compared with the numerical values obtained from

Table 2 Wind tunnel specifications

Type of tunnel	Subsonic, open circuit, suction type
Test section	0.6m x 0.6m x 2m
Maximum velocity	85m/s
Contraction ratio	1:9
Contraction length	2.25 m
Drive	Axial flow fan driven by AC motor with drive speed controller, 15 HP (11 kW), 440 volts

(a)

(b)

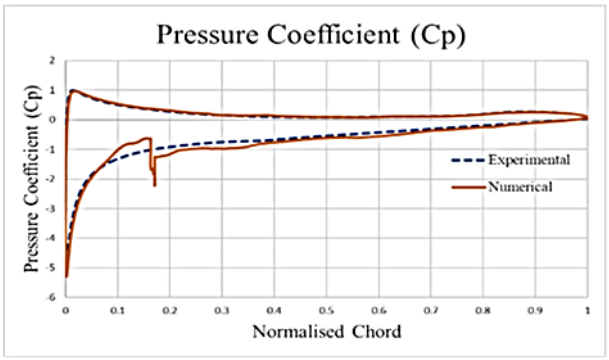

(c)

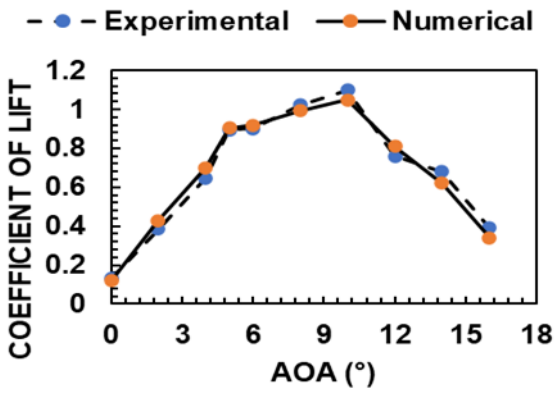

(d)

Fig. 7 Numerical and experimental validation of optimized aerofoil: a) subsonic wind tunnel b) 3D printed optimized aerofoil in test section, c) CP vs. X/C curve, d) coefficient of lift vs. angle of attack curve

the experiments, at a 10° angle of attack, as depicted in Fig. 7. c. The plot of C_P versus the mean chord length curve provided vital insights into the correlation between the experimental data and CFD results. The orientation between the two data sets indicated a high level of consistency, confirming the accuracy and reliability of the computational analysis.

As illustrated in Fig 7.d by the C_L versus alpha (angle of attack) curve, there was clear concordance between the experimental data points and the numerical values derived from the CFD simulations for the baseline aerofoil. This curve, detailing the variation in the lift coefficient with respect to the angle of attack, showing a close match between the experimental outcomes and the CFD simulation data for the baseline aerofoil, substantiates the computational model's accuracy. At moderate angles, such as 5° or 6°, the C_L values can reach approximately 0.5 to 0.7. As the AOA approaches the stall angle, the rate of increase in lift often becomes less steep. This behavior is related to the pre- stall characteristic of an aerofoil. At the stall angle, which can be approximately 12°, the C_L reaches its maximum. For the baseline aerofoil, the peak C_L value could be observed in the range of 1.1 to 1.2, shortly before the stall occurred. Beyond the stall angle, the C_L curve will depict a rapid decline in the lift coefficient value, as the flow separates from the surface of the aerofoil. The experimental work conducted in the wind tunnel, supported the validity of the CFD approach. This validation is pivotal in illustrating the potential for further CFD analyses on aerofoils with dual synthetic jets.

3.2 Grid Independence Study

The study of grid independence was useful in determining the number of elements identified for the optimal mesh density in order to achieve precise and consistent results in our computational simulations. The grid independence study results, as shown in Table 3, provided data about the lift and drag forces. The curves and associated numerical values collectively confirmed that the chosen approach, methodology, meshing parameters, and simulation conditions were indeed conducive

Table 3 Grid independence study values

Mesh Count	Lift Force (N)	Drag Force (N)
207200	145.52	9.43
306360	142.84	9.64
394900	142.93	10.35
426400	142.95	10.43

to a highly accurate representation of the aerofoil's aerodynamic behavior. Based on the study, a mesh count of approximately 400,000 elements was employed for the subsequent analysis

3.3 Pressure Inlet

The effectiveness of circulation control is not determined by the mass of the trailing edge jets, but by their momentum. To ensure an accurate evaluation of the control efficiency, a parameter that can quantify the momentum involved in the process represented by Eq. (2, 3). The momentum coefficient, is the parameter adopted for this purpose, as it represents the ratio of the jet intensity to the free flow intensity and is given by the formula.

$$\text{Coefficient of momentum} = \frac{M_{jet}}{\frac{1}{2}\rho_\infty V_\infty^2 S}, \quad (2)$$

$$\text{where } M_{jet} = \frac{1}{t}\rho_{jet} a_{jet} \int_0^t V_{jet}^2\,(t)\,dt \quad (3)$$

The momentum of the jet is given by M_{jet}; ρ_{jet} and V_{jet} are the density and velocity of the jet; and the area of the jet is given by a_{jet}. The density and velocity of the free stream are given by ρ_∞ and V_∞.

The sinusoidal inlet pressure is a waveform that follows specific mathematical formulations and parameters. This is characterized by a pressure variation, with the maximum pressure of 5000 Pa and the initial pressure value set at 2500 Pa. The amplitude of the sinusoidal waveform, denoted by A, is expressed as $A_0 \sin \omega t$, where Ao, the maximum amplitude, is 2500, and the angular frequency, ω, is determined as $2\pi f^+$, yielding a value of 0.157. The driving frequency, denoted by f, is 40.6, while the characteristic length, represented by l, is 0.007 m. The reduced frequency used for the simulation is given by $f^+ = \frac{fl}{U_\infty}$, and it is 0.025, with the free stream velocity $U\infty$ of 11.27 m/s. The pressure at the inlet is formulated as A0* (sin ωt+Φ), capturing the sinusoidal pressure variation, as shown in Fig. 8.

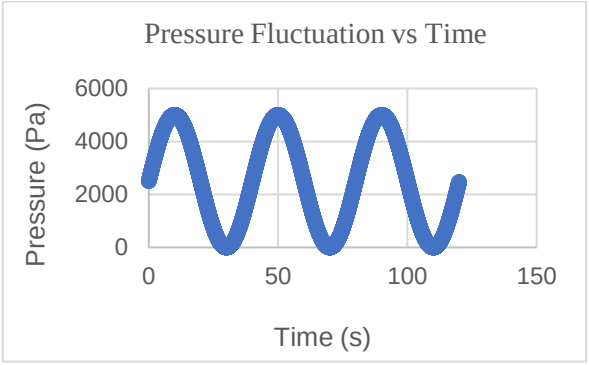

Fig. 8 Fluctuating pressure profile for DSJ

4. RESULTS AND DISCUSSIONS

4.1 Pressure and Velocity Contours

The CFD analyses were conducted for the baseline aerofoil and the aerofoil with DSJs at different angles of attack, solely at positive angles. The analysis was performed at a, sea- level altitude, with a constant reduced frequency of 0.025 and a moment coefficient of 0.2 for both cases throughout. In this study, the aerodynamic forces were systematically assessed across a range of angles of attack, specifically from 0° to 16°, incremented at intervals of 2 degrees. This comprehensive analysis covered a total of eight different angles, providing a detailed understanding of the aerodynamic behavior at each stage. The results for five representative angles of attack, namely 0°, 5°, 10°, 14°, and 16°, are presented in detail.

The angles of attack are categorized into two groups to facilitate a focused discussion of their aerodynamic implications. Angles of 0° and 5° are considered lower angles of attack, where the flow remains largely attached to the aerofoil surface, and the aerodynamic forces are relatively stable. The numerical analysis indicates that both the pressure and velocity contours, along with the aerodynamic efficiency, show minimal variation within this lower range, specifically from 0° to 8°. Conversely, angles of 10°, 14°, and 16° are classified as higher angles of attack. These angles approach and surpass the typical stall angle of the aerofoil, thereby encompassing pre-stall, stall, and post-stall conditions. It is within these higher angles that significant changes in the aerodynamic coefficients become apparent. The study particularly focuses on these conditions because they exhibit marked alterations in the flow characteristics, which are critical in understanding the aerodynamic limits and stall behavior of the aerofoil. The coefficient of pressure curves with respect to the mean chord length, with detailed pressure and velocity contours specifically showcased for 0°, 5°, 10°, 14°, and 16° angles of attack. The pressure inlet values for the DSJ and its fluctuations were calculated at every millisecond from 0 to 120. These values exhibited consistent trends most of the time, with slight variations at every 5 seconds and more substantial changes occurring every 10–15 seconds. Plots and contours illustrating the specified angles of attack are presented for a 10-second interval, providing insights into the efficacy of DSJA application at different angles. The pressure and velocity contours of the baseline aerofoil at 0° AOA are shown in Fig. 9, whereas Fig. 10 showcases the pressure coefficient vs. position curve.

The influence of the DSJ on the flow behavior is not significant at lower angles of attack (0° and 5°), and it does not result in a considerable change or increase in the lift or aerodynamic efficiency. The improvement in circulation around the trailing edge is attributed to the Coanda effect. The pressure and velocity contours at various times, shown in Fig. 11 and 13, demonstrate an increase in the pressure values at the jet exits at 10, 50, and 90 seconds, while reaching minimal levels at 30 and 70 seconds. This pressure fluctuation alters the DSJ's jet exit, impacting the flow near the trailing edge. At 0° and 5° angles of attack,

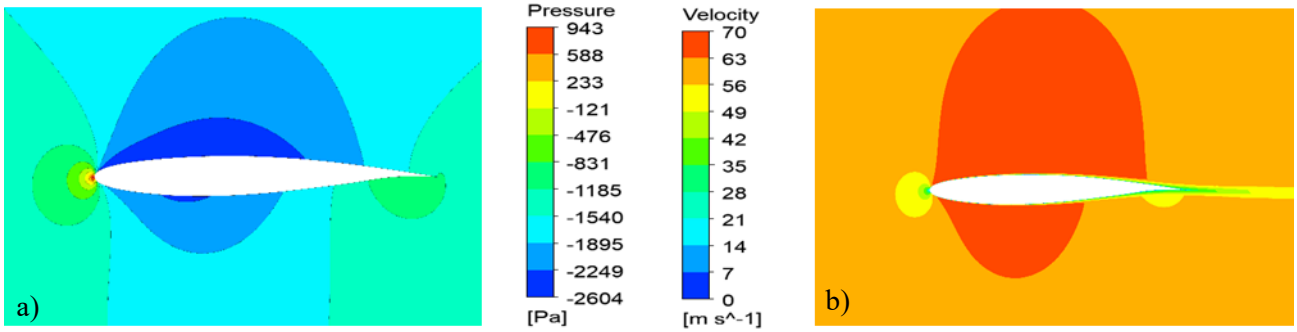

Fig. 9 a) Pressure contour, b) velocity contour of baseline aerofoil at 0° AOA

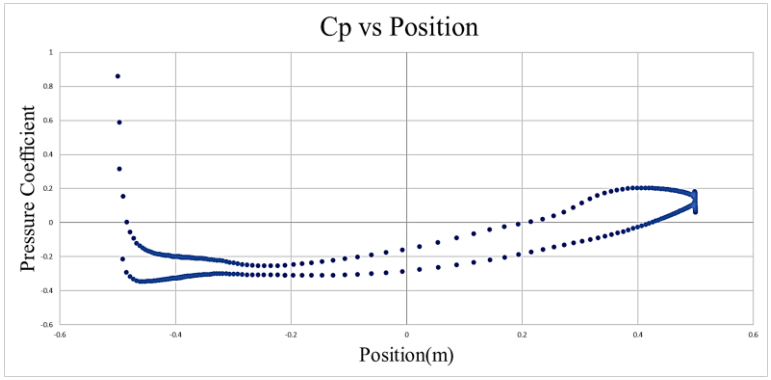

Fig. 10 Cp vs. X/ C curve

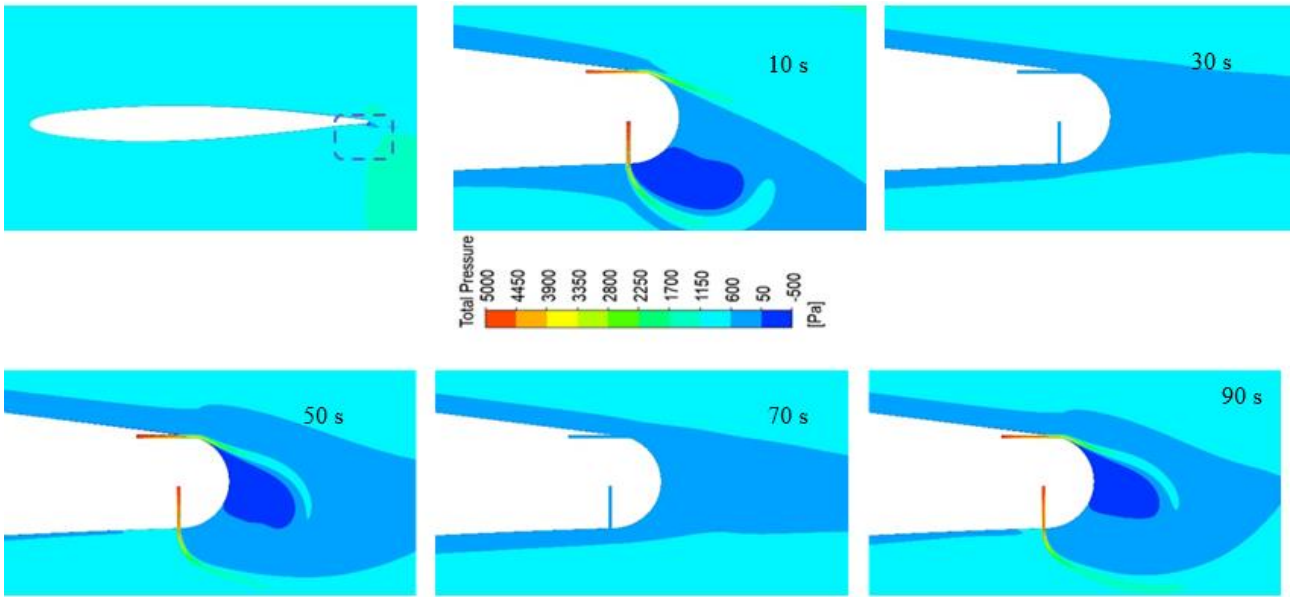

Fig. 11 Pressure contours of aerofoil with DSJ at 0° AOA at 10, 30, 50, 70, 90 seconds (f^+ =0.025)

the pressure and velocity contours show minimal differences between the baseline and DSJ models. However, the wake region, after the trailing edge, undergoes lean changes at these angles. The effectiveness of the DSJA at lower angles is weakened, which is evident in the lift and drag values.

The DSJ generates suction and blowing strokes from its upper and lower parts. At approximately 10 and 50 seconds, at lower angles (0° and 5°), a high jet velocity exit is evident from both the upper and lower trailing edge slots, creating a separation bubble after the trailing edge, as depicted in the velocity contours in Fig. 12 and 14, which significantly affected the aerodynamic characteristics. At 30 and 70 seconds, the impact of the DSJ is negligible and the flow pattern follows the same pattern as in the baseline aerofoil. The velocity contour shows a variation in the location of the stagnation point near the leading edge, influenced by changes in pressure close to the trailing edge due to the synthetic jets. The alteration of the fluid momentum by the synthetic jet near the aerofoil's boundary layer leads to the streamlines bending towards the Coanda surface, a phenomenon known as Coanda deflection.

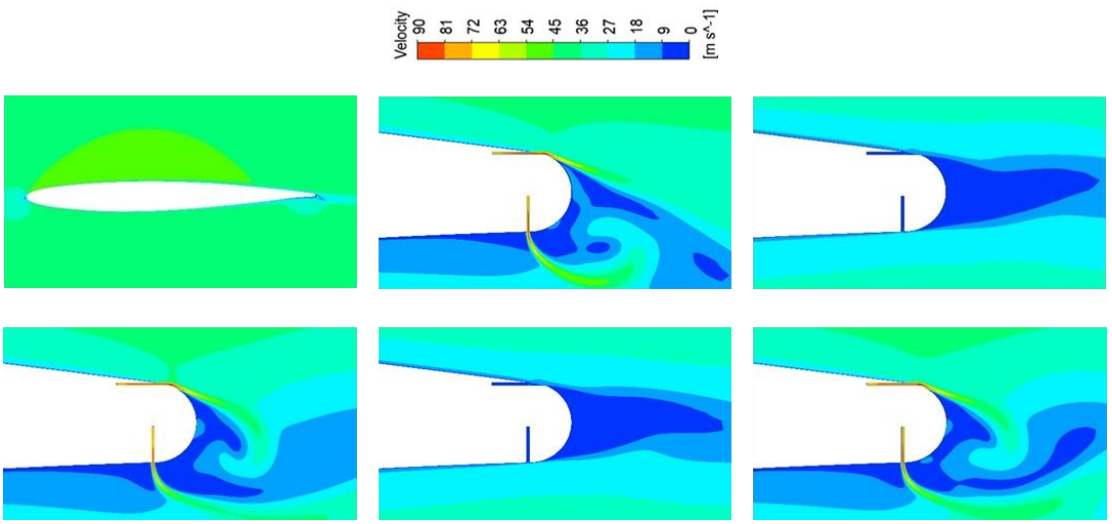

Fig. 12 Velocity contours of aerofoil with DSJ at 0° AOA at 10, 30, 50, 70, 90 seconds (f^+ =0.025)

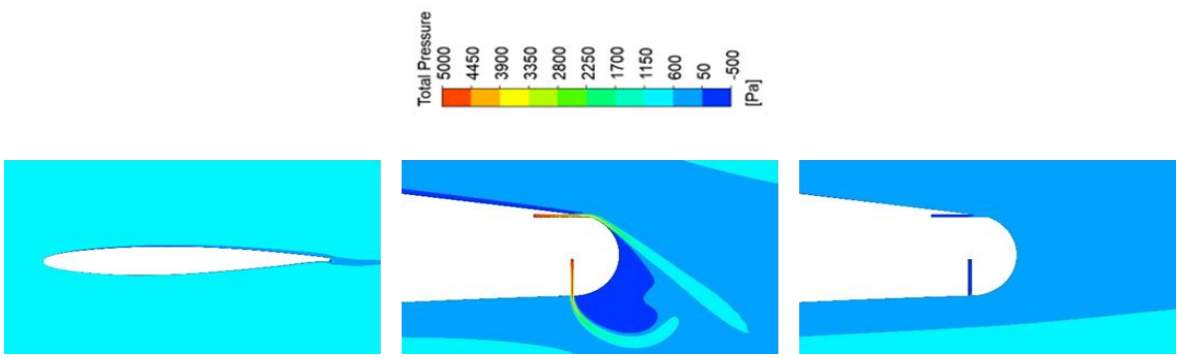

Fig. 13 Pressure contours of aerofoil with DSJ at 5° AOA at 10, 30, 50, 70, 90 seconds (f+ =0.025)

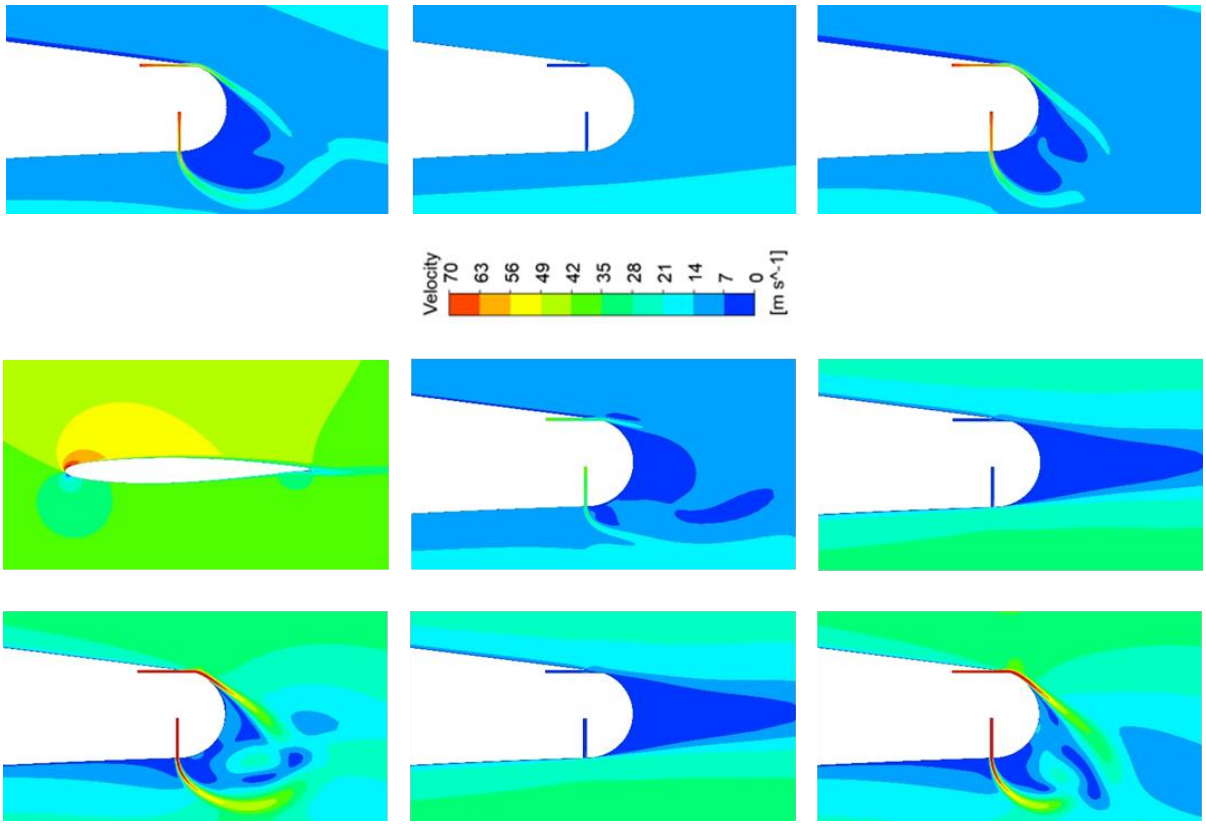

Fig. 14 Velocity contours of aerofoil with DSJ at 5° AOA at 10, 30, 50, 70, 90 seconds (f+ =0.025)

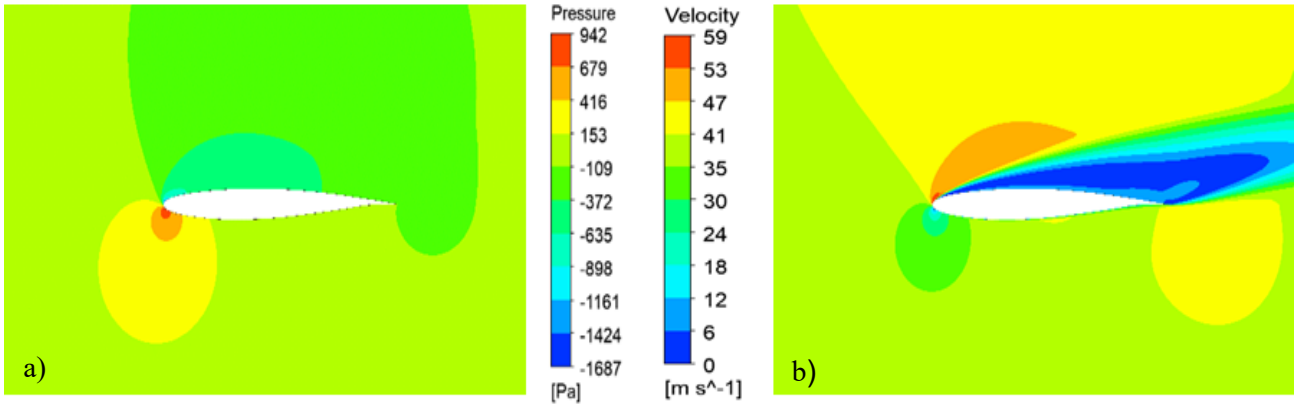

Fig. 15 a) Pressure contour, b) velocity contour of baseline aerofoil at 10° AOA

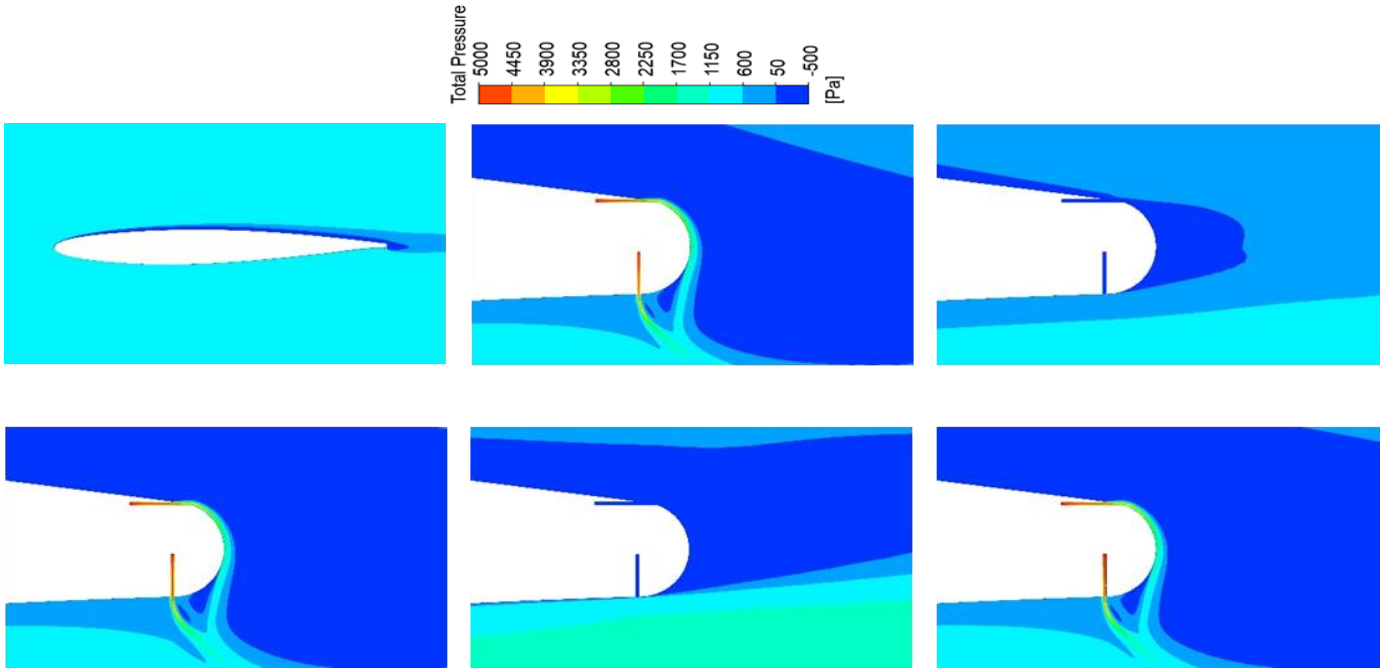

Fig. 16 Pressure contours of aerofoil with DSJ at 10° AOA at 10, 30, 50, 70, 90 seconds (f+ = 0.025)

At higher angles of attack, the influence of the dual synthetic jet (DSJ) becomes noticeable. The critical region stall occurs between 10- and 14-degrees AOA. There is a visible peak in both the circulation control and lift values at these degrees. The initiation of flow separation is observed at around 10 degrees AOA, progressing to a loss of momentum at higher angles. This phenomenon is clearly illustrated by the pressure and velocity contours of the baseline aerofoil in Fig. 15. The velocity contour reveals that streamlines on the suction surface begin to separate, particularly when compared to the pressure surface. The stagnation pressure's position shifts forward to the upper surface, and a noticeable velocity peak contributes to an adverse pressure gradient at higher angles.

At 10, 50, and 90 seconds, the effect of the suction and blowing above and below the surface near the trailing edge is prominent. The circulation control in turn reduces the flow separation zone in the suction surface and attaches the flow closer to the trailing edge. At 30 and 70 seconds, the effect of the jet is very minimal since the pressure fluctuation input drops to zero; this in turn creates a wake zone and separations ahead of the trailing edge, as seen in Fig. 16. However, at 50 and 90 seconds, the change in pressure due to the DSJ causes the flow to gain momentum and reattach to the boundary. The upper trailing curves down and follows the Coanda effect.

At around 10, 50, and 90 seconds, the analysis of the flow field closer to the bottom trailing edge reveals a significant downward deflection due to the influence of the bottom trailing edge jet, which is similar to the action created by a flap deflection. Since no external flaps are used, this effect can be described as a virtual flap. The virtual flap effect due to the jet at the lower or pressure surface can be seen around the trailing edge when the DSJ controls the flow. Additionally, a considerable high-pressure zone appears near the pressure surface trailing edge, enabling positive pressure on the upper trailing edge surface, as seen in Fig. 17. It is significant that, during the pressure blow of the upper trailing edge jet, the fluid velocity near the upper half rises, resulting in the downward deflection of the streamlines. This indicates that the suction stroke at 10, 50, and 90 seconds of the upper half jet enhances the deflection of the streamlines near the lower trailing edge, reinforcing the flap-like deflection. Meanwhile, after 30 and 70 seconds, these

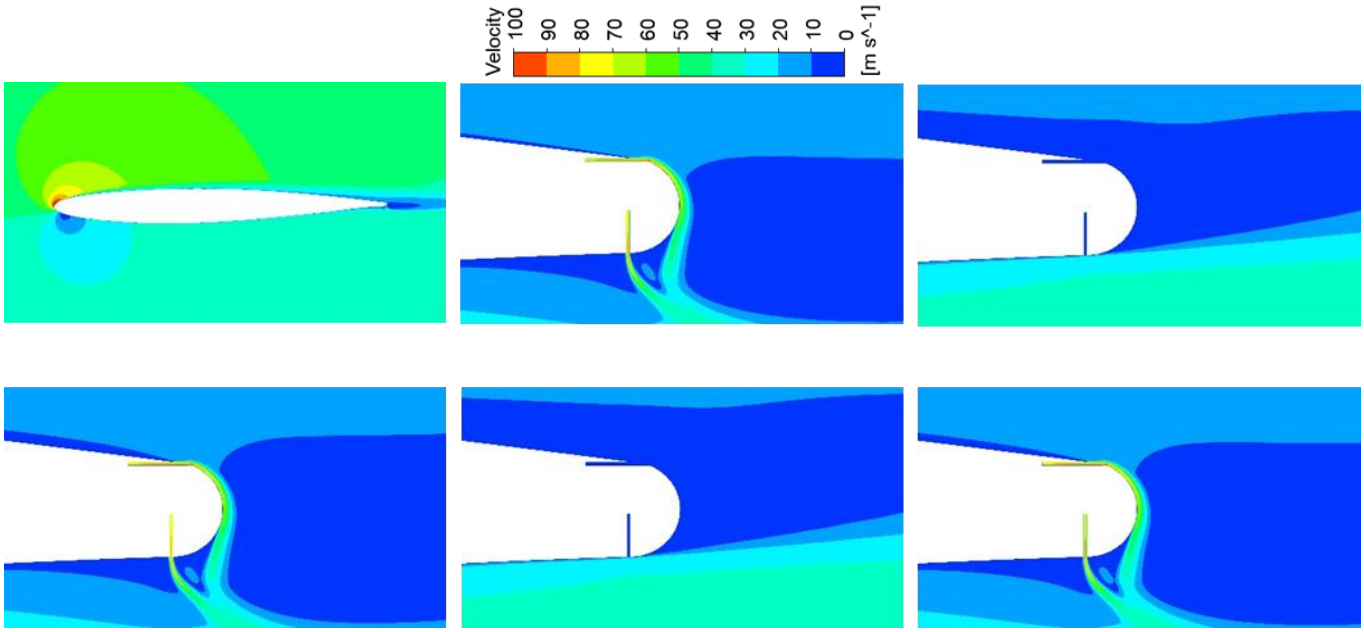

Fig. 17 Velocity contours of aerofoil with DSJ at 10° AOA at 10, 30, 50, 70, 90 seconds (f+ = 0.025)

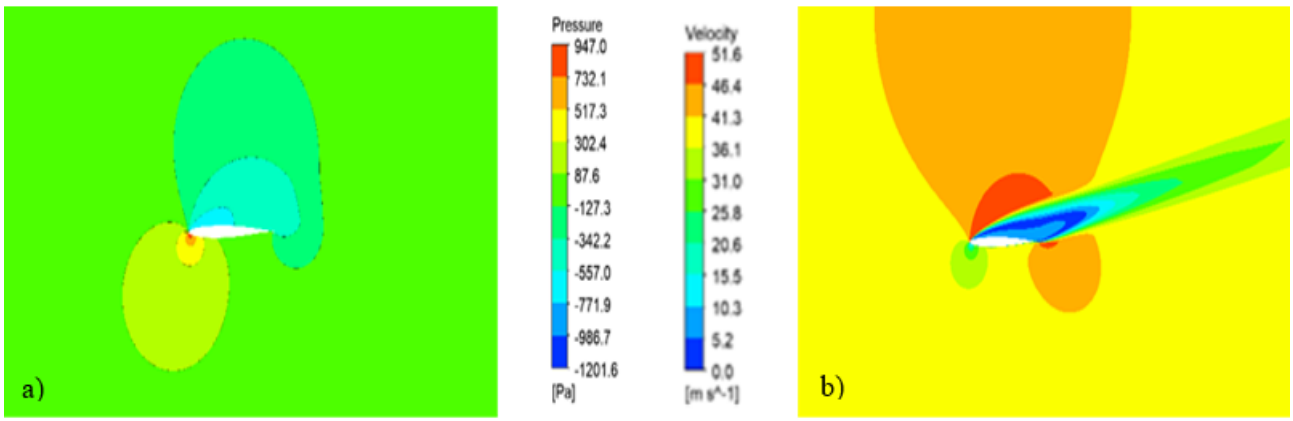

Fig. 18 a) Pressure contour, b) velocity contour of baseline aerofoil at 14° AOA

effects appear lean, where the pressure at the exit of the DSJ gradually decreases with time. The upper and lower trailing edge jets, operating in and out of phase, exhibit a substantial effect at different moments. The bending of the streamlines is more evident considering the complete flow field, representing a combined effect.

At a 14-degree angle of attack, the aerofoil enters the stalling zone, characterized by flow separation, leading to contrasting aerodynamic effects. In Fig. 18, the pressure and velocity contours of the baseline aerofoil illustrate the changes in the pressure and velocity values. The pressure and velocity contours reveal distinctive features on the suction surface of the baseline aerofoil, indicative of a separation bubble's formation. The migration of the stagnation points towards the upper surface and the pronounced velocity peak substantiates the emergence of adverse pressure gradients, signaling the initiation of the stalling of the baseline aerofoil.

From the unsteady aerodynamic CFD analysis, the contours highlight the 'SJ's influence on this critical zone, including the contribution of the change in momentum of the streamlines. The impact of the DSJ at 14 degrees involves a control mechanism producing an anti-phase jet to effectively manage the separation bubble. Through anti-phase jet control, the DSJ moderates the flow separation, suppressing the stall-induced adverse effects. The pressure and velocity contours in Fig. 19 and 20 vividly illustrate how the DSJ changes the formation of the separation bubble, promoting a smoother airflow over the aerofoil. This control mechanism is further augmented by the Coanda effect, observed through the bending of the streamlines towards the bottom surface, enhancing the flow attachment and control. A key advantage of DSJs, when compared to conventional synthetic jets or blowing techniques, lies in their increased energy efficiency. Their ability to exploit the Coanda effect optimizes the fluid flow redirection, thus minimizing the energy consumption. Utilizing the surrounding air, the DSJ emerges as a technologically advanced and environmentally conscious choice for aerodynamic control, particularly during the critical stalling conditions encountered at higher angles of attack.

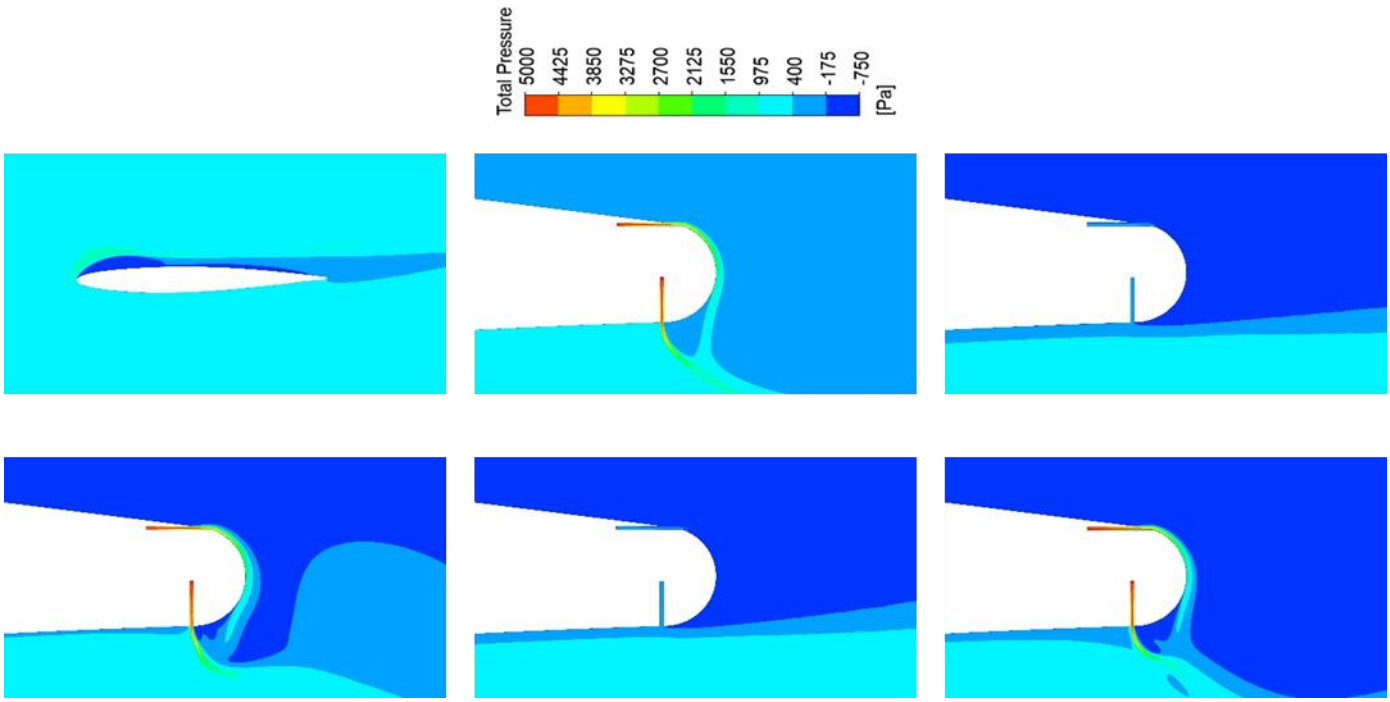

Fig. 19 Pressure contours of aerofoil with DSJ at 14° AOA at 10, 30, 50, 70, 90 seconds (f^+ =0.025)

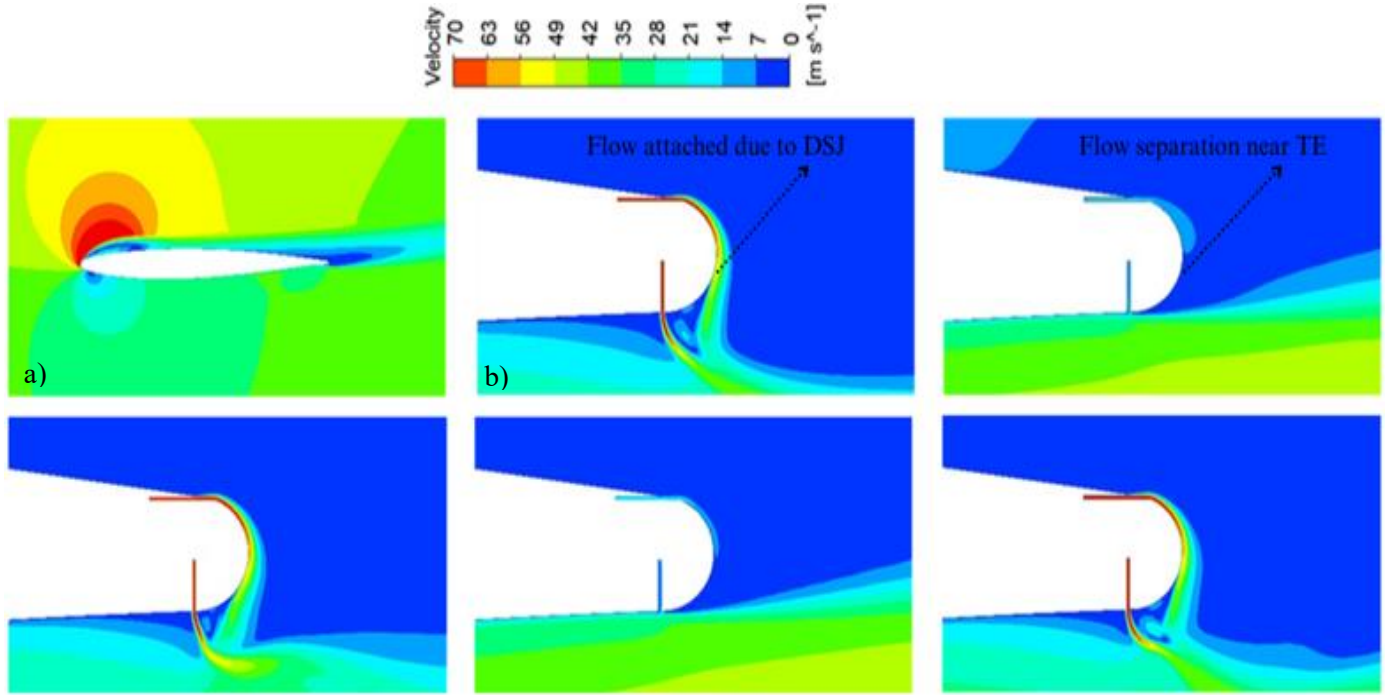

Fig. 20 Velocity contours of aerofoil with DSJ at 14° AOA at 10, 30, 50, 70, 90 seconds (f^+ =0.025)

4.2 Coefficient of Pressure (Cp vs. X/C)

The representation of the *Cp* vs. *X/C* is crucial in detailing the aerodynamic behavior of the optimized baseline aerofoil and the aerofoil with the DSJ at different angles of attack. At higher angles, where aerodynamic challenges such as stall are likely, the *Cp* vs. *X/C* curve provides an insight into improvements in the pressure distribution due to the influence of the DSJ. Figure 21 illustrates the *Cp* vs. *X/C* position of the optimized baseline aerofoil at various angles of attack. Positive values along the upper half of the y-axis signify the pressure surface or the lower side of the aerofoil, while negative values denote the upper surface. At lower angles, the pressure distribution exhibits a smooth curve. The pressure coefficient ranges from -0.5 at a zero angle to approximately -2.5 at 5 degrees, reflecting changes primarily on the upper surface that contribute to enhanced lift values. The pressure remains nearly constant at approximately 1.2 on the lower surface across all angles of attack. As the angle increases, there is a gradual decrease

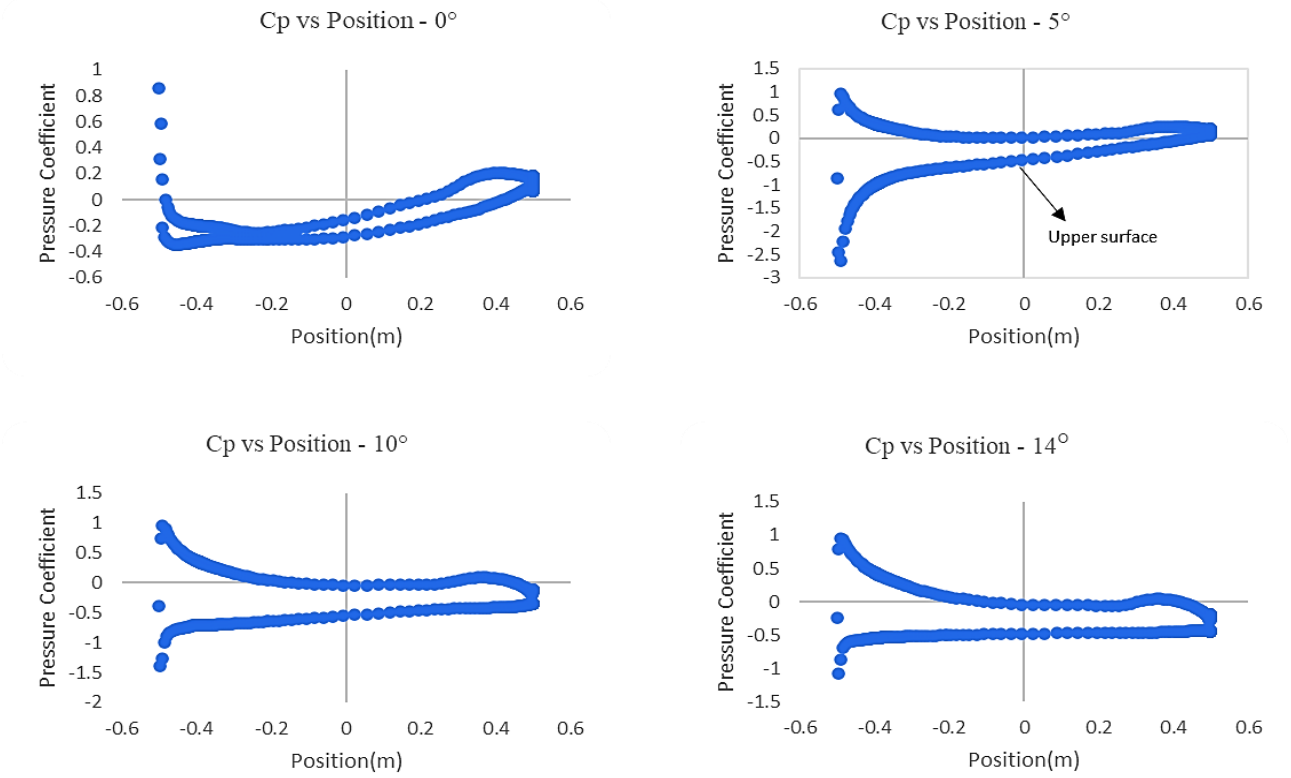

Fig. 21 Coefficient of pressure vs. X/C of baseline aerofoil at various angles of attack

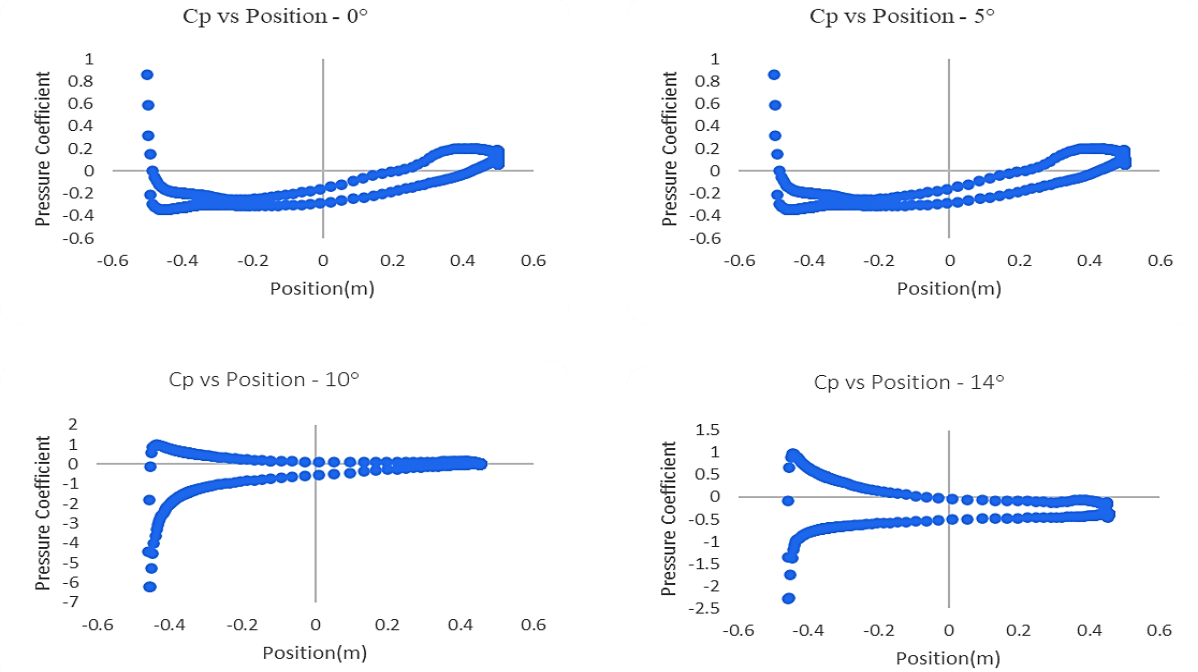

Fig. 22 Coefficient of pressure vs. X/C of aerofoil with DSJ at various angles of attack

in pressure on the upper surface, indicating a positive pressure gradient at 10 degrees and thereby increasing the aerodynamic efficiency. Even with the influence of the DSJ, the *Cp* curves at lower angles affirm the superior performance of the optimized aerofoil.

Contrastingly, although the optimized aerofoil outperforms the original symmetrical design, the introduction of the DSJ further improves the aerodynamic performance at higher angles. Figure 22 illustrates the *Cp* vs. *X/C* position of the aerofoil with the DSJ at various angles of attack. A comparison of the *Cp* vs. *X/C* curves between the modified baseline aerofoil and the one equipped with the DSJ reveals an

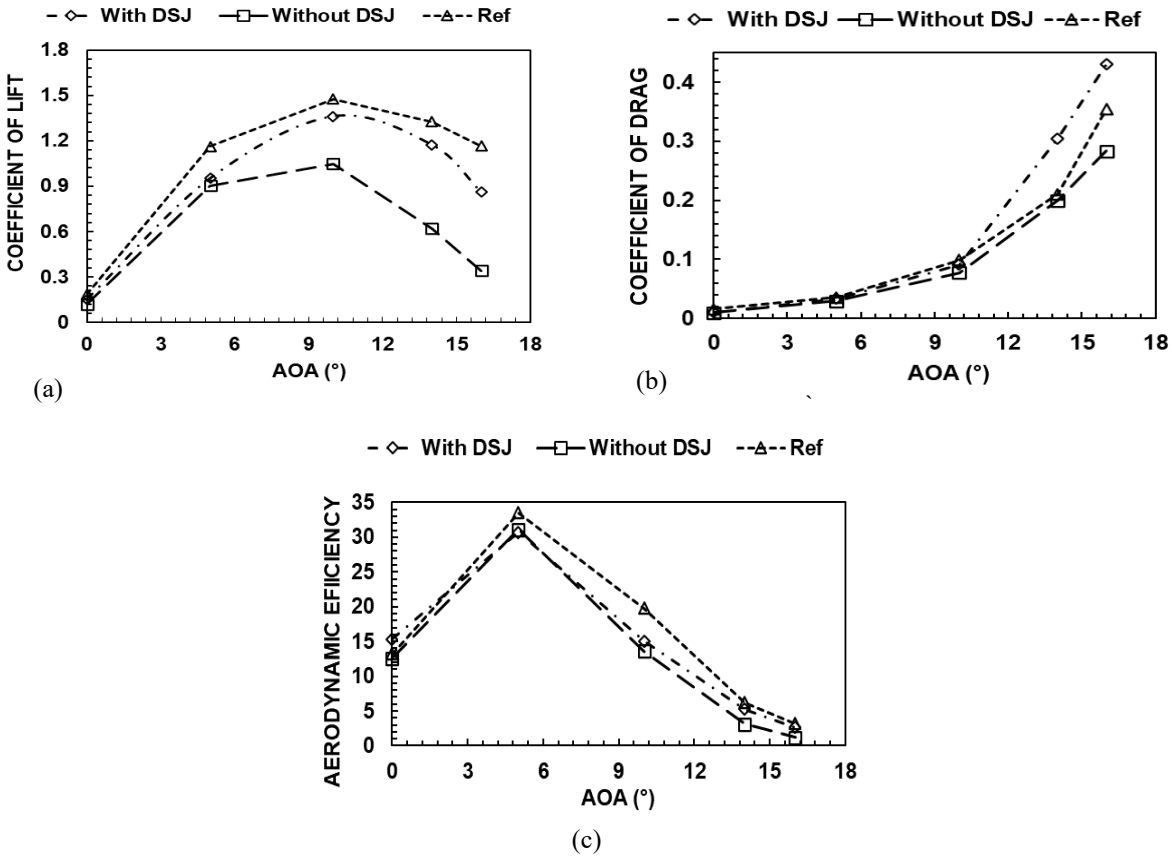

Fig. 23 Comparison of aerodynamic coefficients: a) lift curve, b) drag curve, c) C_L/C_D vs. AOA

enhanced pressure distribution. Notably, at higher angles, particularly around 10 and 14 degrees, identified as stall-prone zones, the pressure differences are amplified. The negative pressure coefficient values for the aerofoil with the DSJ are notably reduced to -6, compared to approximately -3 for the modified aerofoil without the DSJ, at a 10° AOA. Similarly, at a 14° AOA, the pressure coefficient values improve from -1.2 to -2.5. These observations indicate a marked enhancement in the aerodynamic forces at higher angles due to the influence of the DSJ.

4.3 Validation

The application of dual synthetic jet actuators (DSJ) in aerofoils is relatively a new area of research, with limited existing work focusing specifically on this topic. Previous works carried out by researchers employed numerical simulations to predict the aerodynamic impacts of DSJs, with little, if any, experimental validation to support these findings. The present work discusses the effectiveness of dual synthetic jet actuators (DSJs) in the optimized NACA 0012 aerofoil through numerical simulations using CFD. Referring to similar works conducted on the NACA 0015 aerofoil, it uses a similar methodology, focusing on numerical simulations to estimate the aerodynamic performance through coefficients (Li et al., 2022). Despite these differences, the fundamental aerodynamic principles governing the behavior of these aerofoils under DSJs' influence remain consistent due to their symmetric nature. The work carried out by (Hameed & Afaq, 2013) reveals significant similarity in the coefficients of the lift and drag values obtained between the NACA 0012, 0015, and 0018 aerofoils. An investigation of the lift (C_L) and drag (C_D) values across various angles of attack (AOAs) revealed the significant impact of the DSJ on the aerodynamic performance. The C_L values for the DSJ-equipped model exhibited a noticeable increase at higher angles, surpassing the baseline model in Fig. 23. Specifically, at a14- degree AOA, the C_L value for the DSJ model was 1.174, while it was 0.62 for the baseline one. Meanwhile, it rose to 1.32 in the case of the NACA 0015 aerofoil with the DSJ, as shown in the referenced paper. However, at lower angles, such as 0 and 5 AOA, the C_L values showed minimal deviation between the two models.

Examining the C_D values, it is apparent that in the DSJ-induced aerofoil, the rise in lift is followed by a significant rise in drag, especially at higher angles, as seen in Fig. 23. However, the drag is significantly low in case of the NACA 0015 aerofoil, as shown in the referenced paper. The rapid pressure increases near the trailing edge contribute to this surge in drag, potentially affecting the overall aerodynamic efficiency of the aerofoil with the DSJ. This observation suggests that the beneficial effects of DSJ become more pronounced at higher angles, where they enhance the lift but also introduce a substantial increase in drag. To quantitatively assess the efficiency increment brought about by DSJs, an aerodynamic efficiency plot against the AOA was

generated, as shown in Fig. 23. The results indicate a notable rise in aerodynamic efficiency at critical AOAs of 10 and 14 degrees. However, at lower angles (0 and 5 degrees), the efficiency values show a decline.

5. CONCLUSION

The examination of the optimized aerofoil as the baseline configuration, and the incorporation of dual synthetic jet actuators (DSJAs) and Coanda effects, provides compelling insights into the aerodynamic performance across varying angles of attack (AOA). While the baseline aerofoil demonstrates commendable performance at lower angles, the aerofoil equipped with DSJs significantly outperforms it at higher angles, showcasing a remarkable 13.5% increase in aerodynamic efficiency, as opposed to a 7% reduction at lower angles. This notable improvement is attributed to the collaborative influence of the DSJAs and the Coanda surface. The DSJs timely modulation of the pressure over the aerofoil's surface plays a significant role in improving the lift, especially at steeper angles, where flow separation and potential stalling are concerns.

The DSJAs' anti-phase jet mechanism contributes to a relay effect that is particularly effective in lift enhancement. The lower jet's suction stroke amplifies the Coanda effect on the upper side, ensuring that the flow remains attached, even at steep angles. Our findings confirm the value of DSJAs in improving the flight performance in demanding scenarios, such as when aircraft operate at high AOAs. This comprehensive study underscores the potential of DSJs in augmenting the aerodynamic performance, particularly in critical flight conditions at higher angles of attack. The obtained data from the CFD analysis were compared with data on the NACA 0015 aerofoil as a reference. This revealed that the thicker NACA 0015 aerofoil can generate a more significant pressure differential and, hence a higher peak in the aerodynamic coefficients. This comparison highlights the influence of the aerofoil thickness on the effectiveness of DSJAs. The use of DSJAs on an aerofoil or wing surface is advantageous as it allows the active control of the flow, a delay in stall, and an increase in lift without the need for additional mechanical components in the case of passive control devices or surfaces, thereby contributing to a weight reduction and potentially enhancing the fuel efficiency. At the same time, the performance improvement at lower angles of attack is reduced, with minimal deviations in the lift coefficient between the DSJA-equipped aerofoil and the baseline model. Additionally, while DSJAs enhance the lift, they also result in a corresponding increase in drag, particularly at higher angles.

CONFLICTS OF INTEREST

The authors declare no conflicts of interest.

AUTHOR CONTRIBUTIONS

Conceptualization: **Srinath R.** Data Curation and formal analysis: **Srinath R, I Hasan, P. R. Krishnan**. Methodology and Software: **Srinath R, Mukesh R and I Hasan.** Validation and investigation: **Srinath R and Mukesh R.** Project-administration and resources: **Srinath R, Mukesh R and I Hasan**. Visualization: **Srinath R, I Hasan, P. R. Krishnan**. Writing original draft— **Srinath R, Mukesh R**. Writing-review-editing **Srinath R, and Mukesh R**. All authors have read and agreed to the published version of the manuscript.

REFERENCES

Ahmed, R. I., Djojodihardjo, H., Abu-Talib, Abd. R., & Mohd-Rafie, A. (2017). Review on progress and application of active flow control devices-coandă effect on unmanned aerial vehicles. *Pertanika Journal of Scholarly Research Reviews*, *3*(1). 113-137 eISSN: 2462-2028

Ali, H. H., & Fales, R. C. (2021). A review of flow control methods. *International Journal of Dynamics and Control,* 9(4). https://doi.org/10.1007/s40435-020-00730-y

Aqilah, F., Islam, M., Juretic, F., Guerrero, J., Wood, D., & Ani, F. N. (2018). Study of mesh quality improvement for CFD analysis of an airfoil. *IIUM Engineering Journal*, *19*(2). https://doi.org/10.31436/iiumej.v19i2.905

Ball, T., Turner, S., & Marshall, D. D. (2008). Short takeoff performance using circulation control. *46th AIAA Aerospace Sciences Meeting and Exhibit*.

Benard, N., Jolibois, J., Touchard, G., & Moreau, E. (2008 June). A directional plasma-jet device generated by double DBD actuators: an active vortex generator for aerodynamic flow control. In *4th Flow Control Conference* (p. 3763). https://doi.org/10.2514/6.2008-3763

Choudhari, A., Rajendra Jagadale, P., & Chawdhary, A. B. (2021). Computational fluid dynamics, an overview. *International Research Journal of Engineering and Technology*, *08*(09).

Chumbre, V., Rushikesh, T., Umatar, S., & Kerur, S. M. (2018). CFD analysis of airfoil sections. *International Research Journal of Engineering and Technology (IRJET)*, *5*(7).

Dahalan, M. N., Mansor, S., & Ali, M. M. F. (2015). Study the orifice effects of a synthetic jet actuator design. *Jurnal Teknologi*, *77*(8). https://doi.org/10.11113/jt.v77.6160

Djojodihardjo, H., & Thangarajah, N. (2014). Research, development and recent patents on aerodynamic surface circulation control - A critical review. *Recent Patents on Mechanical Engineering*, *7*(1). https://doi.org/10.2174/2212797607666140204004542

Gibert Martínez, I., Afonso, F., Rodrigues, S., & Lau, F. (2021). A Sequential approach for aerodynamic shape optimization with topology optimization of airfoils. *Mathematical and Computational Applications*, *26*(2). https://doi.org/10.3390/mca26020034

Gul, M., Uzol, O., & Akmandor, I. S. (2014). An experimental study on active flow control using synthetic jet actuators over S809 airfoil. *Journal of Physics: Conference Series*, *524*(1). https://doi.org/10.1088/1742-6596/524/1/012101

Hameed, M. S., & Afaq, S. K. (2013). Design and analysis of a straight bladed vertical axis wind turbine blade using analytical and numerical techniques. *Ocean Engineering*, *57*. https://doi.org/10.1016/j.oceaneng.2012.09.007

Hares, H., Mebarki, G., Brioua, M., & Naoun, M. (2019). Aerodynamic performances improvement of NACA 4415 profile by passive flow control using vortex generators. *Journal of the Serbian Society for Computational Mechanics*, *13*(1). https://doi.org/10.24874/jsscm.2019.13.01.02

Hoppe, R. W. (2006). *"Chapter 4: Sequential quadratic programming," Optimization Theory, 2006. [Online]. Available: https://www.math.uh.edu/~rohop/fall_06/Chapter4.pdf*

Ja'fari, M., Shojae, F. J., & Jaworski, A. J. (2023). Synthetic jet actuators: Overview and applications. *International Journal of Thermo fluids* (Vol. 20). https://doi.org/10.1016/j.ijft.2023.100438

Khan, S. A., Bashir, M., Baig, M. A. A., & Ali, F. A. G. M. (2020). Comparing the effect of different turbulence models on the CFD predictions of NACA0018 airfoil aerodynamics. *CFD Letters*, *12*(3). https://doi.org/10.37934/cfdl.12.3.110

Kweder, J., Panther, C., & Smith, J. (2010). Applications of circulation control, yesterday and today. *International Journal of Engineering*, *4*(5).

Larbi, M., Yahiaoui, T., Belkadi, M., Adjlout, L., Ladjedel, O., & Šikula, O. (2020). Numerical study of passive and active flow separation behavior over NACA 0015 airfoil. *International Journal of Fluid Machinery and Systems*, *13*(2). https://doi.org/10.5293/IJFMS.2020.13.2.327

Li, S., Luo, Z., Deng, X., Liu, Z., Gao, T., & Zhao, Z. (2022). Lift enhancement based on virtual aerodynamic shape using a dual synthetic jet actuator. *Chinese Journal of Aeronautics*, *35*(12). https://doi.org/10.1016/j.cja.2022.06.005

Liu, X., Cai, W., Zhang, P., Wang, Y., Huang, Y., & Gao, L. (2022). Study on circulation control of flying wing based on Coanda effect. *Xibei Gongye Daxue Xuebao/Journal of Northwestern Polytechnical University*, *40*(4). https://doi.org/10.1051/jnwpu/20224040845

Kumar, M. S., & Kumar, K. N. (2013). Design and Computational Studies on Plain Flaps. Bonfring *International Journal of Industrial Engineering and Management Science,* *3*(2), 33-39. https://doi.org/10.9756/bijiems.4259

Mamou, M., & Khalid, M. (2007). Steady and unsteady flow simulation of a combined jet flap and Coanda jet effects on a 2D airfoil aerodynamic performance. *Revue Des Energies Renouvelables*.

Mankbadi, R. R., Golubev, V. V., Sansone, M., Sewell, C., & Nguyen, L. (2015). Effect of a synthetic jet actuator on airfoil trailing edge noise. *International Journal of Aeroacoustics*, *14*(3–4). https://doi.org/10.1260/1475-472X.14.3-4.553

Moshfeghi, M., & Hur, N. (2014). *Numerical investigation on the Coanda effect over the S809 airfoil with synthetic jet actuator at high angle of attack.* American Society of Mechanical Engineers, Fluids Engineering Division (Publication) FEDSM, 1B. https://doi.org/10.1115/FEDSM2014-21857

Mukesh, R., Lingadurai, K., & Selvakumar, U. (2012). Application of nontraditional optimization techniques for airfoil shape optimization. *Modelling and Simulation in Engineering*, *2012*. https://doi.org/10.1155/2012/636135

Naqvi, M. A. (2006). *Prediction of circulation control performance characteristics for super STOL & STOL Applications. Georgia Institute of Technology* (Issue December). https://ui.adsabs.harvard.edu/abs/2006PhDT.....77N

Neretti, G. (2016). Active flow control by using plasma actuators. *Recent Progress in Some Aircraft Technologies*. https://doi.org/10.5772/62720

Ou, M., Yan, L., Huang, W., Li, S. bin, & Li, L. quan. (2018). Detailed parametric investigations on drag and heat flux reduction induced by a combinational spike and opposing jet concept in hypersonic flows. *International Journal of Heat and Mass Transfer*, *126*. https://doi.org/10.1016/j.ijheatmasstransfer.2018.05.013

Schwagerus, N., Stößel, M., Krummenauer, M., Kožulović, D., & Niehuis, R. (2023). Numerical investigation of a Coandă-based fluidic thrust vectoring system for subsonic nozzles. *CEAS Aeronautical Journal*, *14*(4). https://doi.org/10.1007/s13272-023-00677-8

Serdar Genç, M., Koca, K., Demir, H., & Hakan Açıkel, H. (2020). Traditional and new types of passive flow control techniques to pave the way for high maneuverability and low structural weight for UAVs and MAVs. *Autonomous Vehicles*. https://doi.org/10.5772/intechopen.90552

Setyo Hariyadi, S. P., Junipitoyo, B., Pambudiyatno, N., Sutardi, & Widodo, W. A. (2023). Aerodynamic characteristics of fluid flow on multiple-element wing airfoil naca 43018 with leading-edge slat and plain flap. *Journal of Engineering Science and Technology*, *18*(1). https://scholar.its.ac.id/en/publications/aerodynamic-characteristics-of-fluid-flow-on-multiple-element-win

Shikhar Jaiswal, A. (2017). Shape parameterization of airfoil shapes using Bezier curves. *Lecture Notes in*

Mechanical Engineering, *PartF9*, 79–85. https://doi.org/10.1007/978-981-10-1771-1_13

Siddiqui, N. A., & Chaab, M. A. (2021). A simple passive device for the drag reduction of an ahmed body. *Journal of Applied Fluid Mechanics*, *14*(1). https://doi.org/10.47176/jafm.14.01.31791

Traub, L. W., & Kaula, M. P. (2016). Effect of leading-edge slats at low Reynolds numbers. *Aerospace*, *3*(4). https://doi.org/10.3390/aerospace3040039

Wang, L., Lu, H., Xu, Y., & Li, Q. (2023). An efficient flow control technique based on co-flow jet and multi-stage slot circulation control applied to a supercritical airfoil. *International Journal of Turbo and Jet Engines*. https://doi.org/10.1515/tjj-2023-0027

Yang, P., Zhu, Y., & Wang, J. (2023). Effect of leading-edge tubercles on the flow over low-aspect-ratio wings at low Reynolds number. *Theoretical and Applied Mechanics Letters*, *13*(1). https://doi.org/10.1016/j.taml.2022.100386

Zhang, J., Du, J., Zhang, M., Chen, Z., Zhang, H., & Nie, C. (2022). Aerodynamic performance improvement of a highly loaded compressor airfoil with coanda jet flap. *Journal of Thermal Science*, *31*(1). https://doi.org/10.1007/s11630-022-1564-2

Zhang, P. F., Yan, B., & Dai, C. F. (2012). Lift enhancement method by synthetic jet circulation control. *Science China Technological Sciences*, *55*(9). https://doi.org/10.1007/s11431-012-4896-4

Zhang, R. rui, Huang, W., Li, L. quan, Yan, L., & Moradi, R. (2018). Drag and heat flux reduction induced by the pulsed counterflowing jet with different periods on a blunt body in supersonic flows. *International Journal of Heat and Mass Transfer*, *127*. https://doi.org/10.1016/j.ijheatmasstransfer.2018.08.066

Zhao, G., Zhao, Q., Gu, Y., & Chen, X. (2016). Experimental investigations for parametric effects of dual synthetic jets on delaying stall of a thick airfoil. *Chinese Journal of Aeronautics*, *29*(2). https://doi.org/10.1016/j.cja.2016.02.010